A Multi-Scale Model of Brain White-Matter Structure and Its Solution from Diffusion MRI

by
Jadrian Miles
Sc. B., Duke University, 2006
Sc. M., Brown University, 2008

A dissertation submitted in partial fulfillment of the
requirements for the Degree of Doctor of Philosophy
in the Department of Computer Science at Brown University

Providence, Rhode Island
September 2010

This dissertation by Jadrian Miles is accepted in its present form by
the Department of Computer Science as satisfying the dissertation requirement
for the degree of Doctor of Philosophy.

Date _____ _____

David H. Laidlaw, Director

Recommended to the Graduate Council

Date _____ _____

John F. Hughes, Reader

Date _____ _____

Ben Raphael, Reader

Date _____ _____

Peter Basser, Reader
NIH

Approved by the Graduate Council

Date _____ _____

Peter Weber
Dean of the Graduate School

Disclaimer

This thesis proposal document is structured to follow the same format as the candidate's eventual dissertation, but in draft form and with many missing pieces, a so-called "dissertation with holes". As such, it is a work of speculation, and many contributions and results are referred to in the text as though they were complete and successful, while the results are in fact yet to be gathered. In particular, none of the development or experiments described in Chapters 2–7 have been completed. Chapter 1, Introduction and Background, nevertheless refers to the expected results for these chapters. This document will undergo extensive revision as development and validation proceed.

In addition, sections that might belong in a thesis proposal but not in a dissertation are attached as appendices. These include Appendix A, "Preliminary Results", and Appendix B, "Projected Timeline".

All prose from this point forward refers to this document as a dissertation rather than a proposal. This is intentional and is meant to reflect the ultimate form of the dissertation.

Abstract of "A Multi-Scale Model of Brain White-Matter Structure and Its Solution from Diffusion MRI" by Jadrian Miles, Ph.D., Brown University, September 2010.

This dissertation describes two primary contributions to the field of medical imaging: a mathematical model of the macroscopic and microscopic structure of the white matter of the human brain; and a technique to compute the parameters of such a model from magnetic resonance imaging scans of a given individual's brain and to evaluate the goodness of fit of the resulting model instance to the available data. The thesis of this work is that combining large- and small-scale structural properties into a single model of the brain white matter allows for an unambiguous solution at both scales that could not be computed using models for each scale in isolation, and that describes the brain more accurately and in more detail than any current technique.

Contents

List of Tables

List of Figures

Chapter 1

Introduction and Background

1.1 Overview

The white matter of the brain is made up of axons that connect different regions of the grey matter to each other and to the body. Axons that connect nearby sites tend to do so along the same path. This gives rise to a higher-level structure of so-called "tracts", and similar tracts group together into "fascicles", many of which have been known to anatomists for many years (see Figure 1.1). Before the mid-1990s, however, the only way to study the anatomical structure of the white matter was with dissection and histology. In the case of human brains, of course, this is what is known as an *ex-vivo* technique: it requires the subject to be deceased.

Diffusion MRI is a magnetic resonance imaging technique that remotely measures water self-diffusion in any chosen direction. Since the fibrous structure of the white matter anisotropically

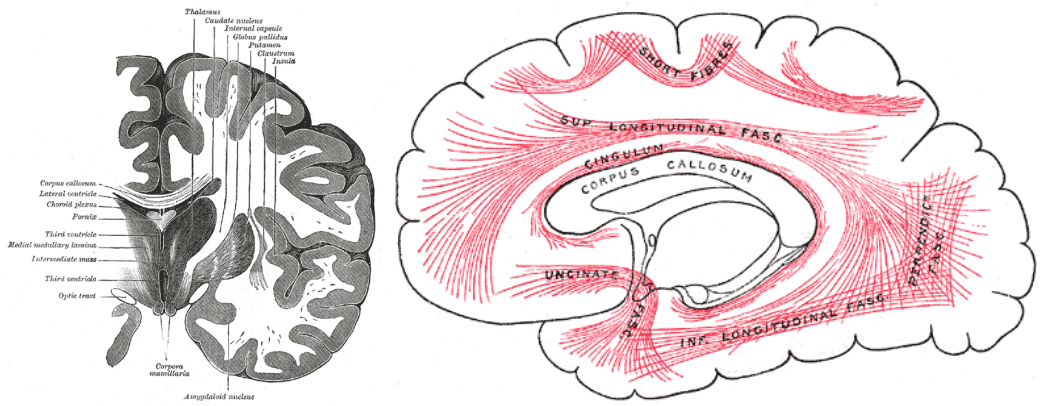

(a) Gray's 718 (b) Gray's 751

Figure 1.1: Plates from the 20th edition of Henry Gray's *Anatomy of the Human Body*, published 1918, illustrating some major white-matter fasciculi.

affects the motion of water molecules, diffusion MRI enables the noninvasive but indirect observation of white-matter structure. In 1994, Basser, et al. [8] described diffusion tensor imaging, the first and still most widely used model for interpreting diffusion MRI data and correlating it to white-matter structure. Since then, many efforts have been made to improve techniques for interpreting diffusion MRI data in terms of white-matter structure, and this dissertation is one such effort.

The output of a diffusion MRI scan is a set of so-called "diffusion-weighted images" (DWIs), which are the principal inputs to the algorithms described herein. Each DWI is a raster volume—that is, a regular three-dimensional grid of voxels, the volumetric analogue of pixels; see Figure 1.2 for two example images. Each voxel in a DWI corresponds to a small volume (generaly 1–2mm cubed) in the space inside the MRI scanner. Models of white-matter structure derived from diffusion MRI therefore generally separate into two regimes: "macrostructure" models that explicitly describe structures larger than a voxel, and "microstructure" models that describe statistical summaries (such as the mean or a simple distribution) of the structural properties of populations of axons in volumes around the size of a voxel. In this context, the macrostructure of the white matter is the shape, orientation, and position of tracts and fascicles. The microstructure of the white matter includes all the structural properties of individual axons: their trajectories, diameters, spacing, permeability, etc., described in aggregate.

The ultimate model described in this dissertation combines macrostructure and microstructure into a single representation, allowing for information at each scale to aid in the solution of the other. Each chapter describes a specific contribution that builds toward the primary contributions listed in the abstract. Chapter 2 describes a geometric model of whole-brain macrostructure derived from diffusion MRI tractography (tractography is explained in §1.5). In this model, each white-matter fascicle is represented by a bounding surface of its volume and a space curve along its medial axis. Chapter 3 describes a method for generating synthetic MR images from the macrostructure model and some simple techniques for adjusting a model instance so that it conforms to known anatomical properties of the brain. Chapter 4 introduces an inverse-solving method for segmenting MR images with the macrostructure model. This method works by iteratively comparing synthetic images of a candidate model instance to the real input images. In Chapter 5 the macrostructure model is used to regularize the solution of established white-matter microstructure models by asserting spatial smoothness of the microstructural properties within each fascicle. Chapter 6 builds on this regularization technique to introduce a novel microstructure model with more parameters (and thus more descriptive power) than the state of the art, which could not be solved without regularization. Finally, Chapter 7 builds on Chapters 4 and 6 to arrive at a combined model of macrostructure and microstructure and an inverse-solving method to fit parameters at both scales simultaneously to the observed data.

1.1.1 Terminology

Throughout this document, certain terms will be used with specific intended meanings. *"Macrostructure"* denotes white-matter fiber trajectories at the millimeter scale as well as the morphology of

the gross segments of brain tissue: coherent white-matter structures and contiguous volumes of grey matter or cerebrospinal fluid. *"WM"*, *"GM"*, and *"CSF"* respectively refer to these tissue and fluid types. The scope of this work is restricted to the brain, and therefore WM and GM refer specifically to the white matter and grey matter of the brain; the spinal cord also contains these tissues, but is primarily excluded from this work. *"Microstructure"* denotes the characteristics of the white matter on a sub-millimeter level, including details of fluid exchange, fluid self-diffusion, and cell geometry. *"Model"* denotes a mathematical model—a set of parameters and a consistent interpretation thereof—while an *"instance"* of that model is a particular set of values assigned to the parameters. *"Inverse solving"* denotes the application of numerical optimization techniques to fit a global model of a system to input observations; this is in contrast to so-called *"forward modeling"* in which the global model results as the aggregation of smaller, independent models that are fit to subsets of the total observations. A *"modeling system"* is the combination of a model and a technique used to fit it to observations. The terms *"axon"*, *"fiber"*, *"tract"*, and *"fascicle"* will refer to the levels of the anatomical heirarchy of the white matter of a real brain, in order of increasing size, while *"curves"* and *"bundles"* are the geometrical representations that will attempt to approximate them in the model.

When describing location and orientation in the brain, special terminology is used. "Left" and "right" are from the subject's perspective, "posterior" means "back" and "anterior" means "front", and "inferior" and "superior" mean "bottom" and "top", respectively. The three orientations of axis-aligned planes also have special names. A "sagittal" plane divides the left-right axis and is parallel to the other two axes; the "mid-sagittal" plane divides the face, head, and brain into symmetrical halves. A "coronal" plane divides the posterior-anterior axis; a coronal plane through the ears, for example, would divide the face from the back of the head. A "horizontal" plane divides the inferior-superior axis; when the subject is standing and looking straight ahead, a horizontal plane is parallel to the ground.

1.2 Brain Structure

The tissue of the human brain is composed of a layer of grey matter around the outside, called the *cortex*, a few internal (or "subcortical") grey-matter structures such as the thalamus and hippocampus, and white matter in the interior. In Figure 1.1(a), GM is rendered in a dark shade, WM in white. There are a small number of cavities in the brain called *ventricles*, which are filled with cerebrospinal fluid (CSF). The brain is divided along the mid-sagittal plane by a large fissure into two approximately symmetrical hemispheres. The hemispheres are connected by a small number of WM fasciculi, primarily the thick band of axons in the center of the brain called the *corpus callosum*.

The cells that transmit signals in the nervous system are called *neurons*. A typical neuron consists of three parts: the cell body; one or more short, branching projections of the body called *dendrites*; and a single long projection called an *axon*, which may have short branches along its length. The *cytoskeleton* of the neuron is composed of microscopic fibers that help maintain the cell's shape, and

in the axon these fibers are typically aligned parallel to the axon itself. Signals travel from the body to the end of the axon in the form of a cascading electrochemical action potential. The interface between the axon of one neuron and a dendrite of another is called a *synapse*, and it is across these synapses that chemical signals may pass to propagate a signal from one neuron to the next.

The brain contains other types of cells in addition to neurons, including glial cells (which provide structural support and biological mainenance to neurons) and the cells of blood vessels. Glial cells produce a structure called *myelin* by wrapping fatty extensions of their cell bodies around short segments of certain axons. An so-called "myelinated" axon is wrapped in myelin along its entire length, forming a *myelin sheath* that increases the propagation rate of the nerve signals along that axon.

Each neuron in the WM of the brain has its body in one location and its distal end in another location, typically several centimeters away. The body of a neuron that transmits signals from a grey-matter site is located close to the interface between the white matter and the grey matter at that site. The distal (far) end of an axon that transmits signals to a grey-matter site is similarly located close to the WM/GM boundary at that site. Thus, apart glial cells, blood vessels, and other cells, the white matter is primarily composed of axons.

If two neuronal bodies near each other have axons that terminate near each other, the axons tend to stay near each other along their lengths, and hence white-matter fibers arise from great numbers of parallel axons that connect different sites together. Individual axons in the human brain white matter typically range from 0.5μm to 20μm in diameter [4], while fiber diameters are on the millimeter scale. Fibers are classified according to what they connect: *projection* fibers connect cortical grey-matter sites to subcortical sites or to the body, *commissural* fibers connect grey-matter sites in opposite hemispheres of the brain, and *association* fibers connect different cortical grey-matter sites in the same hemisphere to each other.

In a given white-matter fiber, then, we can see that axonal membranes, myelin sheaths, and axonal cytoskeleton fibers are all arranged approximately parallel to each other. This restricts the random motion of water molecules both inside and outside the cells, making it easier for water to diffuse *along* the fiber axis than *across* it. Diffusion MRI analysis exploits this anisotropy to detect structural properties of the white matter.

1.3 Diffusion MRI

Each diffusion-weighted image (DWI) that results from a diffusion MRI scan measures water self-diffusion in a chosen direction and over a chosen time scale. The value in a particular voxel in this DWI is a noisy measurement of the average diffusion (in this direction and over this time scale) over the volume of the voxel. Each DWI has two imaging parameters associated with it: a *b-value*, which is related to the time scale, and a *gradient vector*, which dictates the direction. Each DWI in a diffusion MRI acquisition may have a different b-value and gradient vector. Some example DWIs are given in Figure 1.2. There are at least 7 DWIs in an acquisition, often as many as 70, and

sometimes many more.

Let us consider an example acquisition with n DWIs, and a small volume the size of a voxel surrounding a single point in the interior of the brain. This volume has n diffusion measurements associated with it: one for the corresponding voxel in each DWI. Therefore a properly co-registered set of DWIs may be conceived of as a single raster volume whose value in each voxel is a length-n vector, rather than as n separate scalar-valued raster volumes. Each of the n components of the vector in each voxel is a physical measurement of a magnetic resonance response from the nuclei of hydrogen atoms in water as it moves in the volume of the voxel. For an accessible overview of the physics of diffusion MRI, see Mori's review articles from 1999 or 2006 [48, 51]; an excellent in-depth discussion of MRI physics is given in Chapter 17 of Hobbie's medical physics text [32].

The equation for the diffusion MRI signal at b-value b (measured in units of s/mm^2) in a free fluid with diffusion coefficient D (measured in mm^2/s) is

$$S(b) = e^{-bD} S_0$$

This equation is known as the Stejskal-Tanner diffusion equation, named after the authors of the paper that established modern techniques for measuring the diffusion properties of materials using MRI [68].

S_0 is the "unweighted" diffusion MRI response—the signal value at $b = 0$—and depends on fixed tissue properties and imaging parameters. Its equation is $S_0 = \mathrm{PD}(1 - e^{-\mathrm{TR}/T_1})e^{-\mathrm{TE}/T_2}$. A

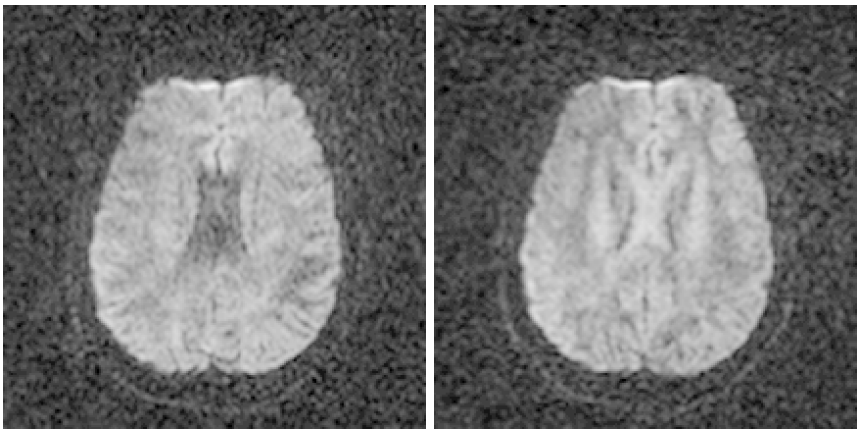

(a) Left-right gradient (b) Anterior-posterior gradient

Figure 1.2: Matching horizontal sections from two DWIs of the same brain, sensitized to diffusion in two different directions. The corpus callosum (CC) is a left-right running band of axons that connects the hemispheres, and its cross-section appears as an X in the centers of these images. Intensity is inversely correlated with diffusion rate, and diffusion is faster along axons than across them. Hence the CC is dark when imaged with a left-right-aligned gradient but light when imaged with a front-back (anterior-posterior) gradient. Other white-matter structures are also evident in intensity differences between these images.

given scanning protocol specifies fixed values for the echo time (TE) and repetition time (TR) of the radio-frequency MRI pulses. Proton density (PD) and the T_1 and T_2 MR relaxation times are physical properties of a material that remain constant over the time span of an MRI scan. S_0 is therefore a constant at any particular position for a given protocol.

The b-value, more formally known as the "diffusion-weighting factor", is a fixed value for a given pulse sequence. b may be computed analytically for simple pulse sequences but it may also be determined experimentally by solving the diffusion MRI signal equation with measurements of a physical sample with known D.

If we take measurements in the same voxel with the same magnetic gradient at two different b-values, say b_1 and b_2, we can compute D, the apparent diffusion coefficient (ADC) in that voxel; as in Figure 1.3, a typical b_1 value is $0\,s/mm^2$.

$$D = -\frac{\ln\left(S(b_1)/S(b_2)\right)}{b_1 - b_2}$$

In neuroscience applications, D is called the "apparent" diffusion coefficient because, when the voxel of interest contains brain tissue, diffusion MRI measures the behavior of water under the influence of the tissue microstructure. Theoretically, the diffusion coefficient of free water is constant at a given temperature. The computed D is therefore the diffusion coefficient that the water *appears* to have when its molecules are hindered and restricted by microscopic structures.

It is important to note that while diffusion MRI can detect the *orientation* of a fascicle by comparing diffusion MR signals, it cannot detect the *direction* of the axons that make it up. This is for a variety of reasons, primarily that the physical principle upon which diffusion MRI is based does not distinguish between water molecules moving parallel to the diffusion gradient vector and

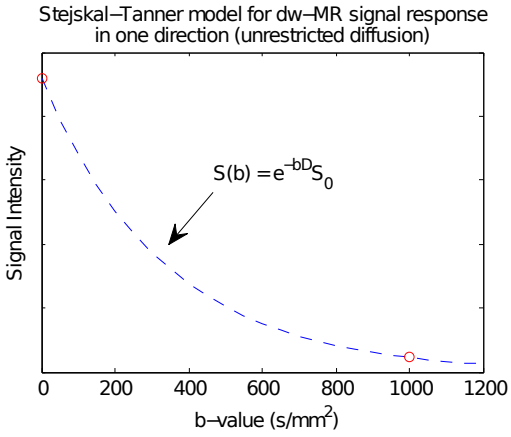

Figure 1.3: An example plot of exponential decay predicted by the Stejskal-Tanner model of the diffusion-weighted MR signal in one direction over a range of b values. Two observations are marked by red circles; the apparent diffusion coefficient is computed by fitting the model to these observations.

molecules moving antiparallel to it. In addition, on the scale of a DWI voxel, water diffusion in the brain is essentially symmetric; that is, there are approximately as many water molecules going in the $+\hat{v}$ direction as there are in the $-\hat{v}$ direction. Lastly, the direction of an axon (that is, which end of it is connected to the neuronal body) does not appear to affect water diffusion in or around the main length of the axon.

1.4 Microstructure Modeling

Among the earliest applications of diffusion MRI in neuroscience was the investigation of WM microstructure properties at the voxel level. The earliest and still most widespread technique for this is diffusion tensor imaging (DTI), which models the anisotropic ADC in each voxel as a second-order tensor and fits it to the orientation distribution of diffusion MRI signals [8]. Visually, the level sets of a three-dimensional second-order tensor are ellipsoids; the three eigenvectors of the tensor correspond to the axes of the ellipsoid, and their corresponding eigenvalues to the lengths of the axes. The DTI model can therefore express a diffusion profile with at most one primary diffusion direction: if one eigenvalue is much larger than the other two, the tensor appears cigar-shaped; if two eigenvalues are much larger than the third, it appears disc-shaped; and if all the eigenvalues are approximately equal, the tensor appears spherical and is deemed *isotropic*.

A variety of measures of the diffusion tensor were developed, including the popular tensor invariant called "fractional anisotropy" (FA) [10]. Especially in clinically-oriented research, voxelwise analysis with DTI, and particularly FA, continues to be the most common use of the technology; e.g., [38, 43, 37, 28]. However, the diffusion tensor model has widely acknowledged disadvantages, such as poor fit in partial volume voxels (where distinct fiber populations or tissue types coexist in the same voxel) and sensitivity to image resolution and other acquisition parameters [2, 57, 70, 3]. FA and other anisotropy measures also suffer from ambiguous interpretation in terms of actual tissue properties; demyelination, axon dropout, and mixed fiber populations, for example, can all cause a decrease in anisotropy [51].

One response to these disadvantages has been the development of mathematical models of the microstructure itself that can be solved directly from the DWIs, e.g., [67, 6, 5, 4]. Parameters of these models include orientation of axon populations, diffusion coefficients of the intra- and extracellular fluid, volume fractions of the various fluid compartments, distribution of axon diameters or "calibers", and, more recently, fluid exchange between compartments [78]. In order to solve these models, however, various assumptions have been made for each—most often that the fibers are oriented in a single, known direction—and none solve for all the parameters listed. In the general case of full-brain diffusion MRI, however, fiber orientation at each point is not known. It has been argued that fluid exchange is also a necessary component of any microstructure model that hopes to accurately approximate the real tissue [53]. Axon caliber affects nerve signal conduction speed [60], making it an important property to be modeled as well. Axon calibers are known to vary widely within the volume of a single voxel in most regions of the WM, implying a need to model

a distribution of calibers, not just a single value [5]. Furthermore, not only do many regions exist where fiber tracts cross, axons even within a single tract exhibit some variability in orientation [36], a property that has as yet not been incorporated into any microstructure model.

As the list of desirable parameters in a microstructure model grows, the system to be solved grows more underdetermined relative to the available diffusion MRI measurements. This author hypothesizes that even if the full four-dimensional probability density function of diffusion were known for a single voxel, a sufficiently detailed but biologically realistic microstructure model could still be underdetermined; that is, that there would exist distinct instances of the model that resulted in the same diffusion profile.

The remedy proposed in this work to these theoretical limitations is the principled application of spatial regularization based on generic, known properties of white-matter tissue. WM axons that terminate inside the brain do so, in healthy brains, only within grey matter [64, 58], and therefore the number of axons in the cross-section of a non-branching fascicle is conserved along its length within the brain. In a given fascicle cross-section with area A, axon volume fraction V, and axon radius distribution $N(r)$, where $\int_0^\infty N(r)\,\mathrm{d}r$ is the total number of axons in the cross-section, then this conservation principle implies $\int_0^\infty N(r)\pi r^2\,\mathrm{d}r = VA$. Since the same axons are members of a fascicle along its entire length, it is also reasonable to assume a fixed (or at least smoothly varying) distribution of radii and intracellular diffusion coefficients, and perhaps even of exchange rates, within a bundle. Whereas the diffusion response in a single voxel may be insufficient to give a unique solution to the microstructure parameters for that voxel in isolation, this dissertation asserts that by incorporating these and other regularizing assumptions into the objective function for fitting microstructure parameters to the diffusion response, a unique optimal solution to the local microstructure model will arise.

The law of large numbers dictates that the distribution of microstructural properties of a population of axons changes smoothly in space, even if the microstructure of each individual axon may change suddenly over a short length scale. This principle holds only if the microstructural changes of axons are spatially independent; that is, a large-scale discontinuity in microstructure properties would be observed if many axons in the same location all had the same change in their individual microstructures at the same location. This phenomenon is not typically observed within individual fasciculi of the white matter, however, justifying the use of spatial regularization within fasciculi.

Many examples exist of previous work on regularizing the solution of diffusion models, both for the diffusion tensor model [19, 74, 55] and for higher-order models [15, 63, 21]. All of these, however, assume equal smoothness of the diffusion field in all directions; that is, when fitting the model in a given voxel in one fascicle, data from a voxel in a different fascicle affect the fit as much as those from a voxel an equal distance away in the same fascicle do. This necessarily leads to blurring of the boundaries between fascicles and between the WM and GM, and therefore exacerbates partial volume issues and the limited resolution of diffusion MRI. The multi-scale model introduced in this work, however, incorporates both the macrostructure and the microstructure, and the corresponding solution technique regularizes microstructure only within bundles, leaving their boundaries sharp at

sub-voxel resolution. This approach is described in Chapters 5, 6, and 7.

1.4.1 Ground Truth for Microstructure

The predictions made by fitting a microstructure model must be validated against some form of ground truth. One form of ground truth is *a priori* knowledge of the microstructure in certain regions; axon radii in regions of the human corpus callosum, for example, are well studied, and the courses of many large fiber tracts are known from anatomical dissection. Another source of ground truth is direct observation of the tissue after scanning, either by dissection and visual inspection or by histology and microscopic inspection. The diamater of a typical white-matter axon is near the diffraction limit of a traditional optical microscope, which puts a theoretical lower bound on the size of features that may be discriminated in the magnified image. Therefore in a light micrograph, while primary axonal orientation may be observed visually and, with the use of specialized stains, the volume fractions of extracellular fluid, myelin, axonal cytoplasm, and other cells may be computed, individual axon radii may nevertheless not be measured with meaningful precision. Confocal and fluorescence microscopy offer higher magnification than traditional optical microscopy, but are moderately more difficult to undertake. Electron microscopy can easily image the micron scale of axons, but is expensive and difficult. These tradeoffs guide the design of experimental validation of microstructure modeling systems.

1.5 Macrostructure Modeling with Tractography

Large-scale and even full-brain macrostructure have also been a subject of investigation with diffusion MRI. The most widely used technique for modeling the WM macrostructure is known as "tractography", in which space curves representing likely paths of fibers through the WM volume are computed from the voxelwise diffusion model instances [9, 50]. A visualizations of an example curve set is given in Figure 1.4. Full-brain sets of tractography curves have been used in fundamental anatomical research of cataloguing the regular structure of the WM fibers [54] and to study cortical connectivity [30]. Manually-selected subsets of curves have also been used as approximations to known WM fascicles in order to study the effects of diseases on specific structures [35]. There is a great deal of variation between subjects in brain morphology [62, 61], indicating that atlases may be insufficient for identifying common structures [79]. Accurate macrostructure reconstruction for each subject individually may therefore offer a better alternative for the comparison of WM structures between subjects [35].

Once again, the best-established diffusion model underlying tractography algorithms is DTI, but it has known disadvantages. The poor fit of the diffusion tensor in partial volume voxels and at fiber crossings can lead simple tractography algorithms to terminate curves prematurely within the WM or to generate curves with spurious redirections into other fiber bundles [41]. In response to the failure conditions of the diffusion tensor model, a number of higher-level diffusion models have also been proposed [12, 33, 70, 31, 69], and research is active on tractography algorithms that take

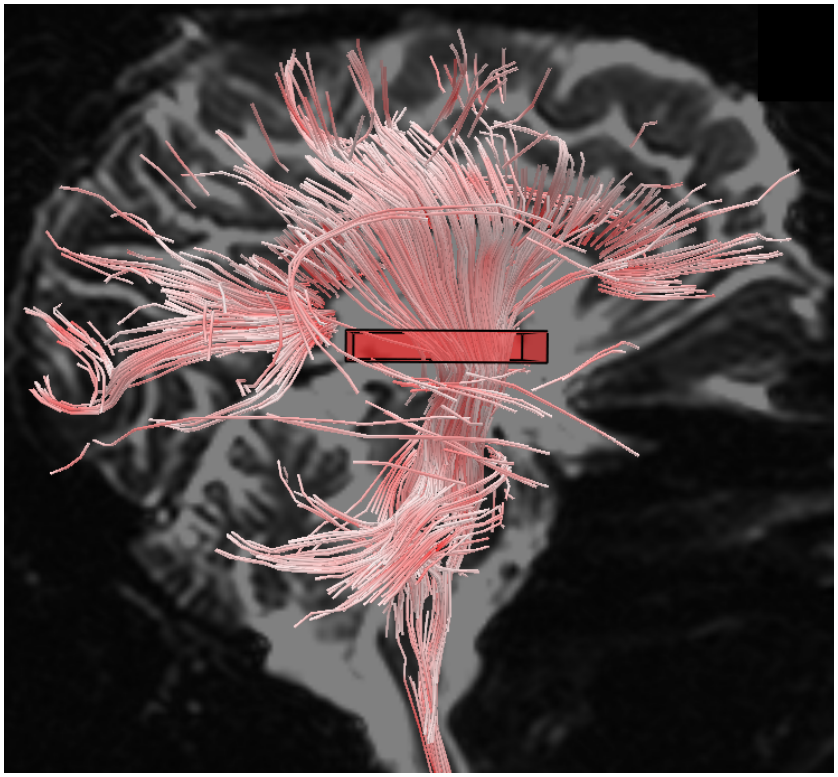

Figure 1.4: DTI-based tractography curves. A subset of a full-brain reconstruction has been selected to show a portion of the right corticospinal tract and a portion of the corpus callosum. The image in the background provides location cues; this is a sagittal view from the subject's right.

advantage of their higher angular resolution [75].

Though more sophisticated tractography algorithms that run on DTI or higher-order models generally perform better than simple ones, they can all result in unrealistic reconstructions. A common failure case is that when fiber tracts cross, a significant number of curves for one tract either terminate at the crossing region, redirect into the other tract, or otherwise lose their directional coherence, while only the remaining fraction successfully pass through to the same tract on the other side of the crossing; e.g., results in [56, 63]. Other techniques appear more successful; e.g., [59, 22]. All of these algorithms improve over traditional DTI-based tractography, however, and any could be incorporated into the method described in this work as a step in the model initialization. (There is also another class of techniques called *probabilistic* tractography that shows promising results for connectivity applications (e.g., [11, 13]) but is not considered in the model described here.)

The solution technique described in this work initializes the macrostructure model by generating a set of curves with tractography and then identifying volumes of coherent WM macrostructure by clustering the curves together. This step is described in Chapter 2. Clustering in general is a fundamental problem in computer science theory [52]. Many options for curve clustering specifically for brain modeling have been investigated in the literature (e.g., Moberts, et al.'s review [47]).

The choice of curve-to-curve similarity measure and clustering algorithm have a strong effect on the resulting clustering, and the large number of curves to be clustered (typically hundreds of thousands) constrains the design of algorithms.

The bounding volumes of clustered curves form the inital values of the model's WM bundles. As these are treated as approximations of WM fascicles, the aforementioned known properties of fascicles may be enforced on them. In order to assert that bundles terminate only within the GM (or at the lower edge of the modeled volume, where the spinal cord projects to the body), the model must also have a reckoning of the GM volume. Another property to be enforced is that any "empty space" in the volume of the brain is occupied by cerebrospinal fluid, which can also be identified with MRI and therefore included in the model. Volumes of GM and CSF are represented in the model by a triangle mesh of their boundaries, which are generated by established tissue classification techniques and isosurface mesh-generation algorithms [39, 66, 61, 65]. Another property that is widely accepted is that the curvature of WM tracts is limited [50, 58, 16], particularly in the interior of the WM; a related but less widely asserted property is that WM fibers are normal to the WM/GM surface where they insert into the GM [71, 45]. In the initialization phase of the inverse solving processes of Chapters 4 and 7, the macrostructure model instance generated by the clustering is directly adjusted so that all WM bundles terminate at the GM and the entire volume of the WM is covered by bundles, further correcting for errors made during tractography; this adjustment is described in Chapter 3. During the iterative optimization, these properties define the space of feasible solutions, and the objective function itself includes terms to favor low bundle curvature and perpendicular insertion of curves into the GM.

Inverse solving has been applied to macrostructure models, specifically tractography, in the past with encouraging results. The "spin-glass" or "spaghetti-plate" tractography model attempts to find curves that terminate only at the WM/GM interface and have low curvature, while still fitting the data as well as possible [44]. It does this by globally minimizing a configuration energy that includes tract curvature and local alignment to the diffusion tensor field and requiring that tracts terminate at the boundary. Recent work has extended this concept to higher-order local diffusion models [26]. The technique described in this work is distinct from these in that it solves for macrostructure and sophisticated microstructure simultaneously (and exploits information at each level to guide the solution of the other), that it models the macrostructure at the level of bundles rather than individual curves, and that it uses the DWIs directly as input rather than working from a higher-level diffusion model.

1.5.1 Ground Truth for Macrostructure

Validation for the output of microstructure modeling systems is based on ground truth analogous to that for microstructure. One form of ground truth is *a priori* knowledge from past study of the anatomy of the brain. Clustering algorithms, for example, are usually compared to manual clusterings prepared by experts with anatomical knowledge [47]. Atlases have been prepared by

merging manual expert clustering or segmentation of a large number of datasets, such as the 81-subject DTI-based atlas of Oishi, et al. [54], and these are also common sources of validation for automatic procedures. The known shapes of difficult-to-reconstruct structures such as the optic chiasm provide challenging test cases for macrostructure modeling algorithms; this is one of the target structures examined in the validation stage of Chapter 2. A less commonly pursued form of ground truth is anatomical dissection. Though the living brain is extremely structurally flexible, it may be fixed for scanning and dissection, allowing for comparison between the shapes of true structures and their reconstructed analogues, as in the analysis of Lawes, et al. [40].

1.6 Significance of Results

Whereas the structure of the white matter could only be studied post-mortem in the past, diffusion MRI now allows for the scientific study of white-matter structure in living brains. The ability to study the white matter *in vivo* has enabled a great expansion in scientific and clinical neuroscience research related to the structure of the brain. Though the analysis of diffusion MRI data is still a maturing field, it has already led to results related to the normal functional connectivity of the brain [30], post-traumatic stress disorder (PTSD) [72, 37], HIV [18], schizophrenia [38, 43, 27], and kleptomania [29]. Structural changes are known from prior post-mortem analyses and other imaging modalities to be associated with brain degeneration in late life [20], and volume decreases in white matter and grey matter (GM) are often used as clinical indicators of brain damage. New discoveries may yet arise from in-vivo white matter imaging; the field is still quite young.

The model and techniques developed in this dissertation give improved reconstruction of neural structure at both the macro- and micro-scale, which will aid neuroscience researchers in investigating the normal structure and development of the brain, the effect of neurodegenerative disorders and other diseases, and the effects of drugs on disease progression. They could also theoretically aid in the diagnosis and prognosis of diseases in clinical settings, although they are very computationally intensive and therefore currently impractical in such settings.

More generally, this dissertation makes contributions to the field of shape modeling for computer vision. The combination of a shape-based spatial segmentation with smooth appearance functions in each segment, along with algorithms for generating such a model from low-level observations and adjusting it to optimize their correspondence, could be useful in modeling other real-world phenomena outside of the field of brain-structure analysis.

Chapter 2

A Geometric Model for Clusters of Diffusion MRI Tractography Curves

2.1 Introduction

This chapter describes a geometric model of clusters of space curves, an energy function for instances of this model, and a technique for clustering curves based on minimizing this energy. This approach differs from established graph-theoretic curve clustering techniques, which model each curve as a node in a complete weighted graph and apply algorithms such as spectral or single-link clustering. The proposed clustering algorithm cannot be expressed as an operation on such a graph, and thereby overcomes some of the limitations of previous techniques at the expense of computational efficiency.

The fundamental notion underlying this model is that a cluster of similar, nearby space curves implicitly describes a volume in space—some curves in the interior of this volume, others on or near its boundary. In diffusion-weighted MRI (DW-MRI) of the brain, advecting from a seed point within the volume of the cingulum, for example, results in a curve that is nearby and approximately parallel to the central axis of this anatomical structure. All seed points in the interior of the cingulum generate similar curves. One use of DW-MRI tractograpy curves, in the absence of a priori knowledge of the location and shape of structures such as the cingulum, is to cluster similar curves together and to use the shape of each cluster as an implicit volumetric segmentation [**?**]. The present technique makes this segmentation explicit by modeling a candidate shape and comparing it to the set of curves it is supposed to represent.

2.2 Model and Algorithms

The clustering algorithm, described in more detail in section 2.2, is modeled after traditional hierarchical or agglomerative clustering [**?**]. The dataset is initialized with each curve forming its own singleton cluster. In each iteration, two clusters are merged together (with a possible simultaneous split) in order to decrease the total energy of the system. A single cluster is represented simultaneously in three ways: by the member curves of the cluster, by a "shrink-wrap" polyhedron that tightly encloses these curves, and by a space curve representing the cluster's medial axis. The energy of a cluster depends on the complexity of the shape of the shrink-wrap polyhedron and medial axis, balanced against the number of member curves.

2.2.1 Shrink-Wrap Polyhedron

The shrink-wrap polyhedron for a set of piecewise-linear curves is related to the alpha-hull of a dense sampling of points on the curves [25], but with the restriction that the polyhedron must be homeomorphic to a sphere. To be more precise, let us define some notation:

- The point-to-curve distance function: $d(p, c) \equiv \min_{q \in c} ||p - q||$.
- The line segment between two points: $\text{seg}(p_1, p_2) \equiv \{(1-\gamma)p_1 + \gamma p_2 \ : \ \gamma \in [0, 1]\}$

For a fixed value α, the shrink-wrap polyhedron for a sufficiently dense set of curves C is a simplicial complex S with certain additional properties:

1. S is a homogeneous 2-complex embedded in $\mathbb{R}^3$ (that is, S is a triangulated surface in 3-space where every triangle's boundary is three edges and three vertices, and every edge or vertex is in the boundary of at least one triangle).
2. $\forall$ vertex $v \in S$, $\exists\ c \in C$ s.t. $v \in c$ (that is, every vertex lies on a member of the curve set).
3. S is without boundary (that is, every edge is the face of exactly two triangles).
4. S is simply connected (combined with the previous property, this implies that the surface segments $\mathbb{R}^3$ into two connected components: a compact "interior" set homeomorphic to a ball, and a non-compact "exterior" set denoted $\tilde{S}$).
5. $\forall\ c \in C,\ c \cap \tilde{S} = \emptyset$ (that is, every curve lies entirely within or on S).
6. $\forall\ c_1, c_2 \in C$ s.t. $c_1 \neq c_2$, $\forall\ p_1 \in c_1,\ p_2 \in c_2$ s.t. $||p_2 - p_1|| \leq \alpha$, $\text{seg}(p_1, p_2) \cap \tilde{S} = \emptyset$ (that is, any line segment shorter than α connecting two different curves lies entirely within or on S).
7. $\nexists$ edge $e \in S$ s.t. $\text{length}(e) > \alpha$ for which it is possible to remove e and its neighbors and patch the resulting hole while satisfying the properties above.

α is a parameter value that is fixed for the entire system. Just as in the case of a classical alpha-hull, setting $\alpha = \infty$ results in the convex hull of all the points in C. An example shrink-wrap polyhedron is illustrated in Figure 2.1(a).

Not all the properties above make sense for small or sparse curve sets. A skeletal curve set C is one for which

$$\exists\ p_1 \in c_1 \in C \text{ s.t. } \nexists\ c_2, c_3 \in C \text{ s.t. } c_1 \neq c_2 \neq c_3 \text{ and } d(p_1, c_2), d(p_1, c_3) \leq \alpha$$

Thus a skeletal curve set is one in which a point exists on some curve for which there are not two other curves that are within α of that point. Therefore enforcing property 7 above could cause points unusually far apart to be connected, and potentially create self-intersections in the surface. The shrink-wrap polyhedron S for a skeletal curve set C satisfies properties 1 and 3–7 above, but replaces property 2 with the following:

2. $\forall$ vertex $v \in S,\ \exists\ p \in c \in C$ s.t. $||v - p|| \leq \epsilon$

for some small constant value ϵ that is fixed for the entire system. This allows for "tubes" of radius ϵ to be constructed around singleton curve sets or segments of curves that are further than α away from all but one other curve (see illustration in Figure 2.1(b)).

2.2.2 Joining and Splitting Clusters

The medial axis for a singleton cluster is the member curve of the cluster. When joining two clusters together,

Draft note: *axes of two clusters should find their overlapping segment, average together, define planes for the ends of the overlap, and finally redefine the average based on the portions of members of the combined cluster that fall between the planes. It might suffice to do a weighted average of the axes. Might have to annotate discontinuities, too, to help the energy function understand what's going on.*

Draft note: *the two end caps of each cluster should also be noted as contiguous regions in the shrink-wrap polyhedron. On the surface of the polyhedron, an end cap is a polygon whose vertices are the end points of member curves.*

2.2.3 Energy Function

Draft note: *Energy function should include axis curvature, axial smoothness of boundary, alignment with trajectories predicted from axis and boundary, "ellipsoidiness" of cross-section, and total length of member curves. Perhaps also total length (or sum of squared lengths) of discontinuities.*

2.2.4 Clustering

Draft note: *The criterion for joining two clusters is whether their combined energy is less than the sum of their separate energies. Heuristics are necessary to determine candidate joins, however. The*

(a) A well-behaved set.

(b) A skeletal set.

Figure 2.1: Sets of space curves and their shrink-wrap polyhedra.

cluster with the longest average length of all its member curves

2.3 Evaluation

Draft note: *This section evaluates the new clustering technique relative to established clustering methods analogously to the Moberts paper.*

2.4 Results and Discussion

Draft note: *Need correspondance measures to expert clusterings.*

The optic chiasm provides well-known challenges to macrostructure models. This structure contains four comingled tracts, two of which cross (or *decussate*), while the other two remain on their respective sides. These mixed fiber populations confound DTI tractography but have been

resolved with tractography over higher-order diffusion models [75]. When initialized with a QBI tractogram, this clustering technique detects each of the four tracts as distinct bundles that overlap in the volume of the optic chiasm, as demonstrated in Figure 2.2.

(a) Anatomical diagram. (b) QBI tracts. (c) Cluster volumes.

Figure 2.2: The optic chiasm. Note that the clustering algorithm detects each of the four tracts as distinct bundles.

2.5 Conclusions

Using a geometric curve bundle model expresses relationships between bundles that cannot be modeled as functions of scalar-valued similarity measures between their member curves. The results demonstrate that this model enables an automatic clustering that more closely matches expert hand-clustering than the state of the art. The output of the algorithm is also useful for other computations, such as tract-specific DTI statistics or geometry-based post-processing, as it explicitly represents the volumes of generated clusters.

Chapter 3

Simulating the Diffusion MRI Response of a Geometric White Matter Tissue Model

3.1 Introduction

This chapter introduces a technique for generating synthetic diffusion MR images from a tissue segmentation accompanied by medial axes of the segments. For cases in which the model does not conform to known properties of brain structures, an algorithm is provided to make naïve adjustments to the model.

Synthetic diffusion MR images have typically been used for two purposes: to create images from computational phantoms for the validation of models against the ground truth of the phantom, and to re-create input data from a model fit to a real dataset to check the goodness of that fit. The present method falls into the latter category, as the model that forms its input is expected to be derived from a real dataset by some method, for example by the one described in Chapter 2. Such a model could, however, also be a convenient form in which to describe computational phantoms.

The work of Close et al. falls into the former category [16]. Their method randomly generates a computational phantom in the form of a space-filling collection of bundles of similar curves at sub-voxel packing densities. A fixed sub-voxel radius creates a virtual tube around each curve, and the curves are packed sufficiently tightly that very little space within a given voxel falls outside of the union of all such tubes. The simulated image arises by subdividing each voxel, classifying which tube contains it, and assigning an axially symmetric diffusion tensor parallel to the associated curve with fixed FA and MD. The tensors are summed to arrive at a single tensor for a synthetic DTI.

Draft note: *this next paragraph is just a placeholder and needs work.*

A more generic technique is that of Leemans et al. [42]. Here, tractography curves are the input,

and a tunable convolution kernel dictates how similarly curve-aligned axially symmetric tensors fade into their surroundings around each curve.

3.2 Methods

3.2.1 Tissue Classification

Draft note: *Classify voxels into contiguous regions of white matter, grey matter, or cerebrospinal fluid using [39, 66, 61]*

3.2.2 Tractography Clustering

Draft note: *reference the previous chapter*

3.2.3 Bundle Adjustment

Even the best tractography methods have well-known shortcomings, in particular when dealing with partial-volume voxels that contain distinct fiber populations or tissues. Such voxels generally fall below the anisotropy threshold for DTI tractography, causing curves to terminate prematurely; when the anisotropy is high enough, partial voluming effects distort the principal eigenvector and spuriously redirect curves into incorrect regions [41]. Higher-order models also fall prey to reduced performance in partial volume regions [56, 63].

The result of tractography errors is that the tissue segments that result from the geometric clustering operation described above do not conform to known generic properties of healthy white matter. Adjusting these bundles to reflect these properties should make them match the imaged brain more accurately in partial-volume regions. The two properties we address are the termination conditions of white-matter fascicles and the space-filling segmentation of brain tissues.

Fascicle Termination

White-matter axons that terminate inside the brain do so, in healthy brains, only within grey matter [64, 58]. Tractography errors at regions of partial voluming between grey and white matter can make bundles terminate a few voxels short of the GM/WM interface, and errors at regions of crossing fibers can make bundles terminate deep within the white matter. We address these cases by growing bundles axially at either end.

To grow a bundle at one end, its medial axis is extended in a straight line segment from that end a given distance d. The direction of the new segment is a weighted vector sum of the tangent vectors of the last $5d$ of the axis. The end cap is detached from the bundle surface, moved to the end of the new axis segment, and the surface is then stitched together with a collar of new triangles. See figure 3.1.

Figure 3.1: Growing a bundle axially. The medial axis (blue) extends in a straight line, and the triangulated surface of the bundle has a "collar" of new triangles (green) parallel to the new axis segment inserted below the end cap (pink).

Draft note: *Grow bundles axially to GM surfaces if they can grow without touching anyone else; join bundles together across gaps if their end caps meet while growing and their axes approximately align. Multiple joins mean a branching bundle, which must be split axially.*

Space-Filling Segmentation

Another known property of the brain is that any "empty space" in the volume of the brain is occupied by cerebrospinal fluid. Therefore, the union of all the bundles in the white-matter model must cover all the voxels classified as white matter by the tissue segmentation.

Draft note: *Grow bundles radially smoothly along their lengths and optimize to fill space with minimal overlap.*

3.2.4 MR Response

Draft note: *Subsample each voxel. If a bundle is not present in a sub-voxel, it gets a default diffusion tensor and S_0 based on its tissue classification. For each bundle in the remaining sub-voxels, compute a diffusion tensor and sum the responses.*

3.3 Evaluation

Our input data were full-brain diffusion MRI scans of 20 healthy volunteers, each with 64 diffusion gradient directions and 10 unweighted images, with 1.8mm isotropic voxels, 70 axial slices, and a 128×128 acquisition matrix. The images were intra-subject coregistered using FSL's FLIRT [34]. Three tractography techniques were applied:

- *Basic DTI:* diffusion tensors were fit linearly and the FACT tractography algorithm [49] applied using the MGH Diffusion Toolkit software [73].
- *Careful DTI:* diffusion tensors were fit nonlinearly by the method of Ahrens, et al. [1] and tracked by 2^{nd}-order Runge Kutta according to the method of Zhang, et al. [76].
- *QBI:* the default q-ball model and 2^{nd}-order Runge Kutta QBI tractography were applied using Diffusion Toolkit.

The output of the Basic DTI tractography method was used to manually create three regions of interest (ROIs) in the left hemisphere of eahc subject, matching the following anatomical features: the crossing region of the tapetum of the corpus callosum and the corticospinal tract; the boundary region between the corpus callosum and the cingulum bundle; and the boundary region between the superior motor cortex and the corticospinal tract. These ROIs highlight partial volume regions of the white matter that are difficult to reconstruct with tractography. Figure 3.2 illustrates the ROIs for one subject. ROIs were selected so that their volumes were approximately equal.

Figure 3.2: Partial volume regions of interest.

We compared the synthetic DWI method described above against the "thickened tractogram" method of Leemans, et al. [42]. In particular, we used the two-parameter "saturated" response model, in which each tractography curve has a saturated core that blends into its neighbors with a gaussian falloff. This method generates a synthetic DTI, whereas we wished to generate synthetic DWIs. We accomplished this by plugging in the b-value and gradient vector into the Stejskal-Tanner diffusion response equation for a tensor-valued diffusion coefficient, which is read in each voxel from the synthetic DTI. The radius of saturation w and the standard deviation of the falloff σ are independent parameters on each curve; as in the original Leemans, et al. publication, we optimized their values to minimize the mean squared difference between the synthetic and input DWIs.

For each of the 60 tractography sets (20 subjects × 3 tractography techniques), each of the two DWI synthesis techniques were applied and the mean squared differences between the synthetic DWIs and the inputs were computed in the voxels classified as white matter in the tissue classification step.

3.4 Results and Discussion

Figure 3.3 shows a summary of the MSD values for the different techniques. In each case, the geometry-based technique performed as well as the others, averaged over the entire white-matter volume. When selecting partial volume regions, however, this technique reconstructed the source DWIs significantly more accurately. Example DWIs showing comparable results in plain white matter and improved results in partial volume regions are shown in Figure 3.4. The average number of voxels in the whole white matter was 97853, while the average per-subject total number in the ROIs was 730.

(a) All WM, Basic DTI. (b) All WM, Careful DTI. (c) All WM, QBI.

(d) PV ROIs, Basic DTI. (e) PV ROIs, Careful DTI. (f) PV ROIs, QBI.

Figure 3.3: Mean squared differences between the simulated and original DWIs, for three tractography protocols and two DWI simulation methods. Blue bars are the Leemans method; green bars are the method from this chapter. The top row of plots are for the entire white-matter volume; the bottom row are for selected partial-volume regions of interest.

3.5 Conclusions

The primary strength of the technique described in this chapter is its use of geometric information about bundles of tractography curves to automatically adjust the bundles to confrom to simple known properties of brain tissue. The results of the above evluation indicate that this adjustment step improves over previous techniques at reconstructing the diffusion MRI signal in partial volume regions, where this task is most difficult.

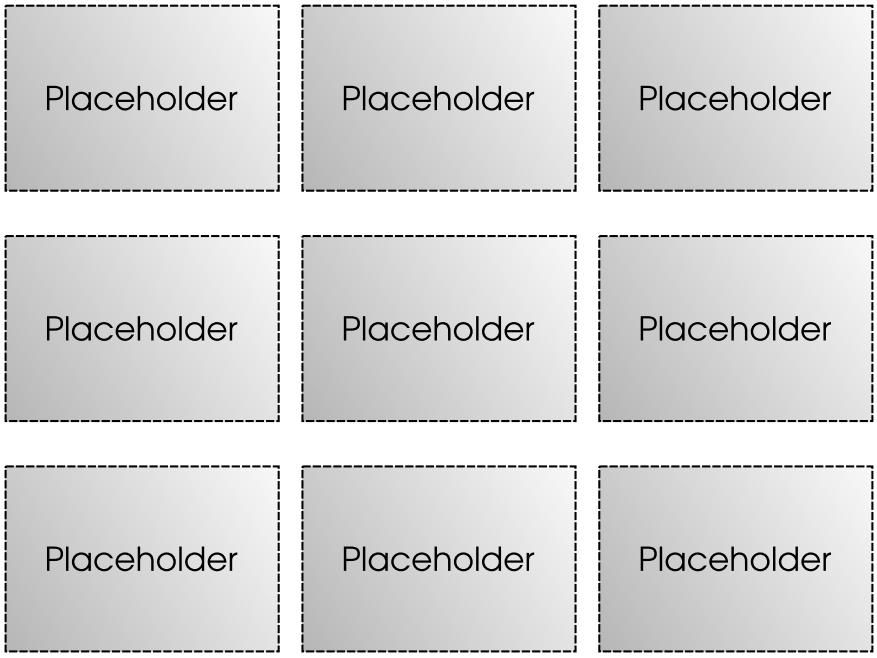

Figure 3.4: Example DWIs illustrating the performance of the different techniques. The center column are the original images, the left column are reconstructions by the Leemans method using QBI tractography, and the right column are reconstructions by the geometric method. The top row is from the crossing ROI, the middle is from the corpus callosum–cingulum boundary, and the bottom is from the motor cortex.

Chapter 4

Automatic Segmentation of Diffusion MR Images with a Geometric White Matter Tissue Model

4.1 Introduction

This chapter describes an automatic method for segmenting diffusion MR images based on a voxelwise tissue classification and an initial tractography-derived white-matter segmentation. The segmentation is a geometric macrostructure model: it describes regions by triangulations of their bounding surfaces and, for white-matter structures, their medial axes. The regions are non-exclusive, to account for crossing-fiber regions. It is possible to generate synthetic DWIs directly from this model, and an iterative method adjusts the segmentation until the synthetic DWIs match the inputs as closely as possible.

4.2 Methods

4.2.1 Tissue Classification and Bounding Surfaces

4.2.2 White Matter Structures

4.2.3 Synthetic DWIs

4.2.4 Shape Optimization

4.3 Evaluation

Draft note: *Evaluate against current techniques relative to expert segmentation. Best would be to use one of Mori's tractography-based atlases and the input data from that. The most common current technique is to just use an atlas and affine (or even spline) transform it. To compare against this we would need our own expert segmentation, or two separate atlases. Maybe divide the subjects from Mori's atlas into two groups, and cross-validate? Also, show an improvement over the output of the previous chapter/paper, relative to same.*

4.4 Results and Discussion

4.5 Conclusions

Chapter 5

Regularizing White Matter Microstructure Models with a Macrostructure Segmentation

5.1 Introduction

This chapter introduces a regularization technique for diffusion models in the white matter of the brain that uses a tract-aware white-matter segmentation to keep the boundaries between neighboring fascicles sharp. This technique is generic and can easily modify most existing regularization methods, while improving results in the partial volume regions where regularization is most important.

Many examples exist of previous work on regularizing the solution of diffusion models, both for the diffusion tensor model [19, 74, 55] and for higher-order models [15, 63, 21]. All of these, however, assume equal smoothness of the diffusion field in all directions; that is, when fitting the model in a given voxel in one fascicle, data from a voxel in a different fascicle affect the fit as much as those from a voxel an equal distance away in the same fascicle do. Draft note: *Is this true? The weighting is probably anisotropic in some cases. Double-check references.* This necessarily leads to blurring of the boundaries between fascicles and between the WM and GM, and therefore exacerbates partial volume issues and the limited resolution of diffusion MRI.

The regularization introduced in this chapter, however, assigns each voxel (or, for multi-population models, each population in each voxel) to a segmentation volume defined by its boundary. This segmentation may be derived from a registered white-matter atlas or from un-regularized tractography. The regularization of each element (voxel or population) is isolated from elements in other segments, no matter how close they are, leaving the boundaries between these segments sharp in the regularized image.

The same technique may also be applied to supersampling, in which case the boundaries between

segments remain sharp at the resulting finer resolution.

5.2 Methods

5.2.1 Macrostructure Segmentation

Custom Atlas

Draft note: *Use either a tractography atlas like Mori's, nonlinearly registered to the subject, or a custom atlas as in Lawes, et al 2008.*

Tractography Clustering

Draft note: *Same technique as in previous chapter.*

5.2.2 Microstructure Regularization

5.3 Evaluation

We performed two evaluations: the first regularizes diffusion tensors using a white-matter atlas, and the second regularizes an AxCaliber [5] multi-population model using a custom segmentation derived from q-ball tractography.

5.3.1 DTI Regularization

Our input data were full-brain diffusion MRI scans of 10 healthy volunteers, each with 64 diffusion gradient directions and 10 unweighted images, with 1.8mm isotropic voxels, 70 axial slices, and a 128×128 acquisition matrix. The images were intra-subject coregistered using FSL's FLIRT [34].

Draft note: *Classify brain tissue regions to get a gross WM segmentation. Compute diffusion tensors three ways: normally, regularized, and regularized by the atlas. Simulate DWIs from each resulting tensor field for comparison to originals.*

5.3.2 AxCaliber Regularization

We imaged an *ex-vivo* macaque brain twice: once with 64 diffusion gradient directions and 2.0mm isotropic voxels, and once with 150 gradient directions and 1.0mm voxels with 8 repetitions. In both cases, the scan volume was 128×128×70mm; for the first imaging protocol, this was acheived with a 64×64 acquisition matrix and 35 slices, while in the second we used a 128×128 acquisition matrix and 70 slices. Total acquisition times were 15 minutes and 160 minutes, respectively.

Both diffusion MRI datasets were coregistered and axially aligned using FSL's FLIRT [34]. We then performed q-ball tractography on both, using the MGH Diffusion Toolkit software [73].

Figure 5.1: Partial-volume regions of interest for DTI regularization.

Guided by the high-resolution tractography, we picked six planar regions of interest in the brain volume with easily identified primary axon orientations. These are illustrated in Figure 5.2. Each ROI was a small slab approximately 5×5×1mm.

1. Along the mid-sagittal plane in the genu of the corpus callosum, in a region identified by tractography as projecting into the prefrontal cortex.

2. Along the mid-sagittal plane in the splenium of the corpus callosum, in a region identified by tractography as projecting into the occipital lobe.

3. Along a sagittal plane in the body of the corpus callosum, in a region identified by tractography as projecting into the postcentral gyri of the parietal lobe, to the left of the mid-sagittal plane, inferior of the cingulum bundle. The superior edge of this ROI extends into the cingulum.

4. Along a coronal plane aligned with ROI #3 in the left cingulum bundle, with the inferior edge of the ROI extending into the corpus callosum.

5. Along a nearly sagittal plane through the crossing region of the tapetum of the corpus callosum and the corticospinal tract in the left hemisphere. This ROI is normal to the major fiber orientation of the tapetum in this region.

6. Along a nearly horizontal plane through the crossing region of the tapetum of the corpus callosum and the corticospinal tract in the left hemisphere. This ROI is normal to the major fiber orientation of the corticospinal tract in this region.

After scanning, we dissected the brain and used anatomical landmarks to locate the regions of interest in the actual brain tissue. We prepared three parallel, staggered histology slices from each ROI.

Draft note: *Cluster and segment tractogram according to previous chapters.*

Draft note: *Run plain, regularized, and segmented-regularized AxCaliber in the ROIs with manual directions at both resolutions.*

Figure 5.2: Known-orientation regions of interest in the macaque brain.

5.4 Results and Discussion

5.4.1 DTI Regularization

Draft note: *MSD comparison of plain, regularized, and segmented-regularized fits in partial-volume ROIs as in chapter 3. Also perform a χ^2 test for overfitting in the WM volume overall.*

5.4.2 AxCaliber Regularization

Draft note: *Compare low resolution results to high-res and histology for plain, regularized, and segmented-regularized fits.*

5.5 Conclusions

These results show that regularization constrained by a white-matter segmentation can improve the fit of both the diffusion tensor model and a state-of-the-art white-matter microstructure model like AxCaliber in partial-volume regions of the brain. Regularization also prevents over-fitting to noise in otherwise easy-to-fit, single-axon-population white-matter regions.

Chapter 6

The Regularized Solution of a Locally Underconstrained White Matter Microstructure Model

Draft note: *Italic text below are all notes.*

Contribution: a microstructure model that improves on the descriptive power of Ax-Caliber and its ilk, along with a macrostructure-based regularization scheme that makes it possible to solve.

Proof: demonstrate that the results match histology and that state-of-the-art methods do not. Also list assumptions that current models make and the new model does not (e.g.,, known orientation, etc.)

Competitors include [67, 6, 5, 4, 78].

6.1 Introduction

6.2 Methods

6.2.1 Microstructure Model

6.2.2 Diffusion Response

Model Ambiguity

6.2.3 Macrostructure-Based Regularization

6.3 Evaluation

We imaged an *ex-vivo* macaque brain twice: once with 64 diffusion gradient directions and 2.0mm isotropic voxels, and once with 150 gradient directions and 1.0mm voxels with 8 repetitions. In both cases, the scan volume was 128×128×70mm; for the first imaging protocol, this was acheived with a 64×64 acquisition matrix and 35 slices, while in the second we used a 128×128 acquisition matrix and 70 slices. Total acquisition times were 15 minutes and 160 minutes, respectively.

Both diffusion MRI datasets were coregistered and axially aligned using FSL's FLIRT [34]. We then performed q-ball tractography on both, using the MGH Diffusion Toolkit software [73].

Guided by the high-resolution tractography, we picked six planar regions of interest (ROIs) in the brain volume with easily identified primary axon orientations. These are illustrated in Figure 6.1. Each ROI was a small slab approximately 5×5×1mm.

1. Along the mid-sagittal plane in the genu of the corpus callosum, in a region identified by tractography as projecting into the prefrontal cortex.

2. Along the mid-sagittal plane in the splenium of the corpus callosum, in a region identified by tractography as projecting into the occipital lobe.

3. Along a sagittal plane in the body of the corpus callosum, in a region identified by tractography as projecting into the postcentral gyri of the parietal lobe, to the left of the mid-sagittal plane, inferior of the cingulum bundle. The superior edge of this ROI extends into the cingulum.

4. Along a coronal plane aligned with ROI #3 in the left cingulum bundle, with the inferior edge of the ROI extending into the corpus callosum.

5. Along a nearly sagittal plane through the crossing region of the tapetum of the corpus callosum and the corticospinal tract in the left hemisphere. This ROI is normal to the major fiber orientation of the tapetum in this region.

6. Along a nearly horizontal plane through the crossing region of the tapetum of the corpus callosum and the corticospinal tract in the left hemisphere. This ROI is normal to the major fiber orientation of the corticospinal tract in this region.

After scanning, we dissected the brain and used anatomical landmarks to locate the regions of interest in the actual brain tissue. We prepared three parallel, staggered histology slices from each ROI.

Figure 6.1: Known-orientation regions of interest in the macaque brain.

6.4 Results and Discussion

6.5 Conclusions

Chapter 7

A Multi-Scale Model of Brain White Matter Structure and Its Solution from Diffusion MRI

Draft note: *Italic text below are all notes.*

Contribution: the combined macro and micro model, along with the full inverse-solving method.

Proof: comparison to competitors relative to histology and dissection / block face imaging / expert segmentation of anatomical images.

7.1 Introduction

7.2 Methods

7.3 Evaluation

7.4 Results and Discussion

7.5 Conclusions

Appendix A

Preliminary Results

While this proposal describes plans for work that has not yet been undertaken or completed, several examples of preparation indicate the feasibility of the proposed research and the candidate's capability to undertake it.

Curve Clustering

A review of existing curve-to-curve similarity measures [17, 14, 77, 23] determined that these were insufficient for the goal of exploiting broken tractography curves to recover more complete tract clusters in a full-brain clustering. A new measure was developed that mimics the "corresponding segment" measure of [23, 24] for arbitrary pairs of curves, and weights the similarity by the evenness of the correspondence to bias against skewed curve pairs. A parallel algorithm for efficient computation of the sparse similarity matrix was designed and implemented. Well-known problems with the overzealous clustering behavior of agglomerative methods such as that described in [77] were anticipated, and a combined strategy that includes spectral clustering [52] was investigated but ultimately abandoned. This work was presented in an invited talk at the NIH Sectionon Tissue Biophysics and Biomimetics in May 2009 entitled *A Specialized Inter-Curve Similarity Measure for Agglomerative Diffusion MRI Streamline Clustering.* The similarity measure and corresponding segment calculations are re-used in the geometrical clustering algorithm of Chapter 2.

Collaborations

Established collaborations exist between the candidate's research group (headed by Dr. David Laidlaw) and medical researchers around the world, in which Dr. Laidlaw's group provides DTI data processing and implements new computational techniques, while the outside collaborators provide raw data and pursue their own research agendas. The candidate has also collaborated directly with researchers at other institutions on work relevant to the proposed research.

- **Stephen Correia, Ronald Cohen, Stephen Salloway, and Win Gongvatana (Butler Hospital, Miriam Hospital, and Brown University, Providence, RI):** The teams led by Drs. Correia, Cohen, and Salloway have contributed more than 100 diffusion MRI scans at 1.5T and 3T to Dr. Laidlaw's research group over several years, and have collected more than 100 new scans at 3T and high angular resolution for a current study of HIV. In turn, this research group has collaborated with them on several clinical studies and the development of new analysis techniques. Since 2007, the candidate has worked closely with Dr. Correia's team to provide software tools for DWI processing and to troubleshoot mathematical issues with data analysis.

- **Edward Walsh and Michael Worden (Brown University):** The candidate has worked with Drs. Walsh and Worden to design a high angular resolution diffusion MRI acquisition protocol and, with other members of Drs. Correia and Laidlaw's groups, to refine the standard diffusion MRI research protocol used across labs at Brown. He has also trained with the technical staff at the medical imaging center at Brown to participate in planning and carrying out MRI acquisitions of human volunteers.

- **Gregory Balls and Lawrence Frank (University of California, San Diego):** The candidate negotiated with Drs. Balls and Frank to extend the functionality of their Monte Carlo diffusion simulator, DifSim [7], to work with more detailed microstructure. Licensing issues ultimately aborted this line of development.

- **Bruce Spottiswoode (University of Stellenbosch, Cape Town, South Africa):** The candidate has been the primary contact at Brown on data processing issues for a Cape Town research team studying HIV and has developed new software to accommodate their data. This project is led by PI Robert Paul of St. Louis, Missouri and was granted funding by the NIH in 2009.

- **Mark Bastin (University of Edinburgh):** The candidate has coordinated processing of brain tumor data for this collaborator.

- **Robert Paul and Tom Conturo (University of Missouri, St. Louis):** The candidate has worked directly with the St. Louis-based PIs of a multi-site study of cognitive aging and has developed new software to accommodate their data.

- **Jack Simon (VA Hospital, Portland, Oregon):** The candidate met with Dr. Simon to coordinate further research collaboration with Dr. Laidlaw's group on multiple sclerosis.

- **John Donoghue and Kaivon Paroo (Brown University):** The candidate assisted in technical aspects of the design and analysis of diffusion MRI data for surgical planning in macaques.

- **David Badre and Jennifer Barredo (Brown University):** The candidate was involved in preliminary planning of research collaboration with Dr. Laidlaw's group on multi-modal

detection of functional brain circuits, and provided technical assistance in the analysis of diffusion MRI data.

- **Jeff Chi-Tat Law and Mark Schnitzer (Stanford University):** The candidate was involved in preliminary planning of future research collaboration with Dr. Laidlaw's group on visualization and analysis of brain networks.

Through these collaborations the candidate has gained familiarity with the medical context of the proposed research, including the realities of data acquisition, anatomical and biological knowledge of the brain, and the questions that are investigated with diffusion MRI. Several collaborations afford the re-use for this research of data and software that have already benefitted from substantial effort on the part of the collaborators. The involvement of established medical researchers in this project also encourages clinical applications for the proposed research.

Diffusion Processing Pipeline

Data received from all of the above-listed collaborators are processed by the same "DTI pipeline": conversion of the DWIs to an in-house format, followed by resampling, nonlinear tensor-fitting, tractography, and visualization. Since joining this group, the candidate has expanded the variety of data formats handled by this software pipeline; prior to this work, data only from the Providence-based team could be automatically processed. He has also coordinated the growing list of collaborator data handled by this group and has organized both the data and the software tools involved.

Familiarity with this data pipeline has given the candidate first-hand experience with the variety of data formats and scanning protocols that must be managed, as well as other caveats of real medical data including noise, distortions, metadata ambiguities, and the real-world computational scale of theoretical algorithms.

DTI Protocols

The candidate has assisted Dr. Correia's research group in studying systematic variation in data sets due to different acquisition protocols for DTI. Familiarity with sources of noise and error, as well as established contact with Dr. Walsh and others at Brown's imaging facility, will assist in the design of thorough stability tests for the proposed techniques.

DTI Interpolation

The candidate presented a study on tradeoffs in the interpolation of DTI-derived tensor measures at the ISMRM '09 poster session [46]. This study investigated the practical results of the formal properties of diffusion tensors, and motivates the pursuit of resolution-independent WM models.

Probabilistic Index of Connectivity

Previous research by the candidate into diffusion simulation over diffusion MRI datasets covered a somewhat different area of the diffusion processing literature, including closed-form techniques based on heat diffusion and simulation techniques that fall under the heading of probabilistic tractography. This broader knowledge of the field will assist the candidate in responding flexibly to unanticipated difficulties in the proposed research.

Appendix B

Projected Timeline

The following schedule is based around submissions to conferences and journals, the short names of which are explained below the timeline.

1. **2010 September 29:** 1-page abstract of Chapter 5, *Regularizing White Matter Microstructure Models with a Macrostructure Segmentation*, ready for submission as poster or talk to ISMRM 2011.

2. **2010 November 10:** 1-page abstract of Chapter 2, *A Geometric Model for Clusters of Diffusion MRI Tractography Curves*, ready for submission as poster or talk to ISMRM 2011.

3. **2010 December 20:** Complete draft of Chapter 2, *A Geometric Model for Clusters of Diffusion MRI Tractography Curves*, ready for submission to MRM, NeuroImage, or Vis.

4. **2011 February 15:** Abstract of Chapter 3, *Simulating the Diffusion MRI Response of a Geometric White Matter Tissue Model*, ready for submission as poster to MICCAI 2011.

5. **2011 May 1:** Complete draft of Chapter 5, *Regularizing White Matter Microstructure Models with a Macrostructure Segmentation*, ready for submission to MRM or NeuroImage.

6. **2011 August 1**: Complete draft of Chapter 4, *Automatic Segmentation of Diffusion MR Images with a Geometric White Matter Tissue Model*, ready for submission to HBM, MRM, or NeuroImage.

7. **2011 September 1**: Complete draft of Chapter 6, *The Regularized Solution of a Locally Underconstrained White Matter Microstructure Model*, ready for submission to MRM or NeuroImage.

8. **2012 March 1**: Complete draft of Chapter 7, *A Multi-Scale Model of Brain White Matter Structure and Its Solution from Diffusion MRI*, ready for submission to NeuroImage.

9. **2012 May 1**: Dissertation submitted to the University.

The long gap between submissions 7 and 8 is to accommodate inevitable slipping of any prior submissions. The relevant conferences follow an approximately six-month cycle, allowing for submissions that miss the intended deadline to be submitted to a different venue in about six months.

Submission Targets

- **ISMRM** is the International Symposium on Magnetic Resonance in Medicine, the largest conference in this field. ISMRM accepts only 1-page abstracts, as either talks or posters. Its annual submission deadline is in early November.
- **Vis** is the IEEE Visualization conference, the proceedings of which are published as a special edition of the journal *IEEE Transactions on Visualization and Computer Graphics*. Vis accepts both full papers (as talks) and posters. Its annual submission deadline is in late March.
- **MICCAI** is the Medical Image Computing and Computer Assisted Intervention conference, the proceedings of which are published as Springer Lecture Notes in Computer Science. MICCAI accepts both full papers (as talks) and posters. Its annual submission deadline is in early March.
- **MRM** is the journal *Magnetic Resonance in Medicine*.
- **NeuroImage** is a journal.
- **HBM** is the journal *Human Brain Mapping*, which focuses more on theoretical and computational contributions than do MRM or NeuroImage.

Bibliography

[1] Eric T. Ahrens, David H. Laidlaw, Carol Readhead, Celia F. Brosnan, and Scott E. Fraser. MR microscopy of transgenic mice that spontaneously aquire experimental allergic encephalomyelitis. *Magnetic Resonance in Medicine*, 40(1):119–132, July 1998.

[2] Andrew L. Alexander, Khader M. Hasan, Mariana Lazar, Jay S. Tsuruda, and Dennis L. Parker. Analysis of partial volume effects in diffusion-tensor MRI. *Magnetic Resonance in Medicine*, 45(5):770–780, 2001.

[3] Daniel C. Alexander. *Visualization and Processing of Tensor Fields*, chapter An introduction to computational diffusion MRI: the diffusion tensor and beyond, pages 83–106. Springer, Berlin, 2005.

[4] Daniel C. Alexander. A general framework for experiment design in diffusion MRI and its application in measuring direct tissue-microstructure features. *Magnetic Resonance in Medicine*, 60(2):439–448, 2008.

[5] Yaniv Assaf, Tamar Blumenfeld-Katzir, Yossi Yovel, and Peter J. Basser. AxCaliber: A method for measuring axon diameter distribution from diffusion MRI. *Magnetic Resonance in Medicine*, 59(6):1347–1354, 2008.

[6] Yaniv Assaf, Raisa Z. Freidlin, Gustavo K. Rohde, and Peter J. Basser. New modeling and experimental framework to characterize hindered and restricted water diffusion in brain white matter. *Magnetic Resonance in Medicine*, 52(5):965–978, 2004.

[7] Gregory T. Balls and Lawrence R. Frank. A simulation environment for diffusion weighted MR experiments in complex media. *Magnetic Resonance in Medicine*, 62(3):771–778, 2009.

[8] Peter J. Basser, James Mattiello, and Denis LeBihan. MR diffusion tensor spectroscopy and imaging. *Biophysical Journal*, 66:259–267, Jan 1994.

[9] Peter J. Basser, Sinisa Pajevic, Carlo Pierpaoli, Jeffrey Duda, and Akram Aldroubi. In vivo fiber tractography using DT-MRI data. *Magnetic Resonance in Medicine*, 44(4):625–632, 2000.

[10] Peter J. Basser and Carlo Pierpaoli. Microstructural and physiological features of tissues elucidated by quantitative diffusion tensor MRI. *Journal of Magnetic Resonance*, 111:209–219, 1996.

[11] T.E.J. Behrens, H. Johansen Berg, S. Jbabdi, M.F.S. Rushworth, and M.W. Woolrich. Probabilistic diffusion tractography with multiple fibre orientations: What can we gain? *NeuroImage*, 34(1):144–155, 2007.

[12] T.E.J. Behrens, M.W. Wollrich, M. Jenkinson, H. Johansen-Berg, R.G. Nunes, S. Clare, P.M. Matthews, J.M. Brady, and S.M. Smith. Characterization and propagation of uncertainty in diffusion-weighted MR imaging. *Magnetic Resonance in Medicine*, 50(5):1077–1088, 2003.

[13] Jeffrey I. Berman, SungWon Chung, Pratik Mukherjee, Christopher P. Hess, Eric T. Han, and Roland G. Henry. Probabilistic streamline q-ball tractography using the residual bootstrap. *NeuroImage*, 39(1):215–222, 2008.

[14] Anders Brun, Hae-Jeong Park, Hans Knutsson, and Carl-Fredrik Westin. Coloring of DT-MRI fiber traces using laplacian eigenmaps. In *Proc. EUROCAST*, volume 2809 of *Lecture Notes in Computer Science*, pages 564–572, 2003.

[15] Yunmei Chen, Weihong Guo, Qingguo Zeng, Guojun He, B. Vemuri, and Yijun Liu. Recovery of intra-voxel structure from HARD DWI. In *Proceedings of IEEE International Symposium on Biomedical Imaging*, pages 1028–1031, April 2004.

[16] Thomas G. Close, Jacques-Donald Tournier, Fernando Calamante, Leigh A. Johnston, Iven Mareels, and Alan Connelly. A software tool to generate simulated white matter structures for the assessment of fibre-tracking algorithms. *NeuroImage*, 47(4):1288–1300, October 2009.

[17] Isabelle Corouge, Sylvain Gouttard, and Guido Gerig. Towards a shape model of white matter fiber bundles using diffusion tensor MRI. In *Proc. IEEE ISBI*, pages 344–347, April 2004.

[18] Stephen Correia, Stephanie Lee, Thom Voorn, David F. Tate, Robert Paul, Song Zhang, Stephen P. Salloway, Paul F. Malloy, and David H. Laidlaw. Quantitative tractography metrics of white matter integrity in diffusion-tensor MRI. *NeuroImage*, 42:568–581, 2008.

[19] Olivier Coulon, Daniel C. Alexander, and Simon R. Arridge. A regularization scheme for diffusion tensor magnetic resonance images. In *Proc. 17th IPMI*, volume 2082 of *Lecture Notes in Computer Science*, pages 92–105, Berlin, 2001. Springer.

[20] Christos Davatzikos and Susan M. Resnick. Degenerative age changes in white matter connectivity visualized *in vivo* using magnetic resonance imaging. *Cerebral Cortex*, 12(7):767–771, Jul 2002.

[21] Maxime Descoteaux, Elaine Angelino, Shaun Fitzgibbons, and Rachid Deriche. Regularized, fast, and robust analytical Q-ball imaging. *Magnetic Resonance in Medicine*, 58(3):497–510, 2007.

[22] Maxime Descoteaux, Rachid Deriche, and Alfred Anwander. Deterministic and probabilistic Q-ball tractography: from diffusion to sharp fiber distribution. Technical Report 6273, INRIA Sophia Antipolis, Valbonne Sophia Antipolis, France, August 2007.

[23] Z. Ding, J.C. Gore, and A.W. Anderson. Case study: reconstruction, visualization and quantication of neuronal fiber pathways. In *Proc. IEEE Vis.*, pages 453–456, 2001.

[24] Zhaohua Ding, John C. Gore, and Adam W. Anderson. Classification and quantification of neuronal fiber pathways using diffusion tensor MRI. *Magnetic Resonance in Medicine*, 49:716–721, 2003.

[25] Herbert Edelsbrunner and Erst P. Mücke. Three-dimensional alpha shapes. *ACM Transactions on Graphics*, 13(1):43–72, January 1994.

[26] P. Fillard, C. Poupon, and J.-F. Mangin. Free-spin tracking: A novel global tractography algorithm. In *Proc. 17th ISMRM*, 2009.

[27] K.J. Friston and C.D. Frith. Schizophrenia: a disconnection syndrome? *Clinical Neuroscience*, 3(2):89–97, 1995.

[28] Jon E. Grant, Stephen Correia, and Thea Brennan-Krohn. White matter integrity in kleptomania: A pilot study. *Psychiatry Research: Neuroimaging*, 147(2–3):233–237, Oct 2006.

[29] Jon E. Grant, Stephen Correia, and Thea Brennan-Krohn. White matter integrity in kleptomania: A pilot study. *Psychiatry Research: Neuroimaging*, 147(2–3):233–237, Oct 2006.

[30] P. Hagmann, L. Cammoun, X. Gigandet, R. Meuli, C.J. Honey, V.J. Wedeen, and O. Sporns. Mapping the structural core of human cerebral cortex. *PLoS Biology*, 6(7), 2008.

[31] Christopher P. Hess, Pratik Mukherjee, Eric T. Han, Duan Xu, and Daniel B. Vigneron. Q-ball reconstruction of multimodal fiber orientations using the spherical harmonic basis. *Magnetic Resonance in Medicine*, 56(1):104–117, 2006.

[32] Russell K. Hobbie. Magnetic resonance imaging. In *Intermediate Physics for Medicine and Biology*, chapter 17. Springer-Verlag, 3rd edition, 1997.

[33] Tim Hosey, Guy Williams, and Richard Ansorge. Inference of multiple fiber orientations in high angular resolution diffusion imaging. *Magnetic Resonance in Medicine*, 54(6):1480–1489, 2005.

[34] M. Jenkinson, P.R. Bannister, J.M. Brady, and S.M. Smith. Improved optimisation for the robust and accurate linear registration and motion correction of brain images. *NeuroImage*, 17(2):825–841, 2002.

[35] Derek K. Jones, Marco Catani, Carlo Pierpaoli, Suzanne J.C. Reeves, Sukhwinder S. Shergill, Michael O'Sullivan, Pasha Golesworthy, Phillip McGuire, Mark A. Horsfield, Andrew Simmons, Steven C.R. Williams, and Robert J. Howard. Age effects on diffusion tensor magnetic resonance imaging tractography measures of frontal cortex connections in schizophrenia. *Human Brain Mapping*, 27(3):230–238, 2006.

[36] Jason A. Kaufman, Eric T. Ahrens, David H. Laidlaw, Song Zhang, and John M. Allman. Anatomical analysis of an aye-aye brain (daubentonia madagascariensis, primates: Prosimii) combining histology, structural magnetic resonance imaging, and diffusion-tensor imaging. *Anatomical Record*, 287A(1):1026–1037, November 2005.

[37] Minue J. Kim, In Kyoon Lyoo, Seog Ju Kim, Minyoung Sim, Namkug Kim, Namhee Choi, Do-Un Jeong, Julie Covell, and Perry F. Renshaw. Disrupted white matter tract integrity of anterior cingulate in trauma survivors. *Neuroreport*, 16(10):1049–1053, Jul 2005.

[38] Marek Kubicki, Robert McCarley, Carl-Fredrik Westin, Hae-Jeong Park, Stephan Maier, Ron Kikinis, Ferenc A. Jolesz, and Martha E. Shenton. A review of diffusion tensor imaging studies in schizophrenia. *Journal of Psychiatric Research*, 41(1-2):15–30, 2007.

[39] David H. Laidlaw, Kurt Fleischer, and Alan Barr. Partial-volume Bayesian classification with voxel histograms. In *Handbook of Medical Image Processing*, pages 195–211. Academic Press, 2001.

[40] I. Nigel C. Lawes, Thomas R. Barrick, Vengadasalam Murugam, Natalia Spierings, David R. Evans, Marie Song, and Chris A. Clark. Atlas-based segmentation of white matter tracts of the human brain using diffusion tensor tractography and comparison with classical dissection. *NeuroImage*, 39:62–79, 2008.

[41] Mariana Lazar, David M. Weinstein, Jay S. Tsuruda, Khader M. Hasan, Konstantinos Arfanakis, M. Elizabeth Meyerand, Benham Badie, Howard A. Rowley, Victor Haughton, Aaron Field, and Andrew L. Alexander. White matter tractography using diffusion tensor deflection. *Human Brain Mapping*, 18(4):306–321, 2003.

[42] A. Leemans, J. Sijbers, M. Verhoye, A. Van der Linden, and D. Van Dyck. Mathematical framework for simulating diffusion tensor MR neural fiber bundles. *Magnetic Resonance in Medicine*, 53(4):944–953, 2005.

[43] Kelvin O. Lim, Maj Hedehus, Michael Moseley, Alexander de Crespigny, Edith V. Sullivan, and Adolf Pfefferbaum. Compromised white matter tract integrity in schizophrenia inferred from diffusion tensor imaging. *Archives of General Psychiatry*, 56(4):367–374, Apr 1999.

[44] J.-F. Mangin, C. Poupon, Y. Cointepas, D. Rivière, D. Papadopoulos-Orfanos, C. A. Clark, J. Régis, and D. Le Bihan. A framework based on spin glass models for the inference of anatomical connectivity from diffusion-weighted MR data — a technical review. *NMR in Biomedicine*, 15(7–8):481–491, 2002.

[45] Jennifer A. McNab, Saâd Jbabdi, Sean C.L. Deoni, Gwenaëlle Douaud, Timothy E.J. Behrens, and Karla L. Miller. High resolution diffusion-weighted imaging in fixed human brain using diffusion-weighted steady state free precession. *NeuroImage*, 46:775–785, 2009.

[46] Jadrian Miles, Ronald Cohen, and David H. Laidlaw. Tradeoffs in supersampling of dti metrics. In *Proceedings of ISMRM*, 2009.

[47] Bart Moberts, Anna Vilanova, and Jarke J. van Wijk. Evaluation of fiber clustering methods for diffusion tensor imaging. In *Proc. IEEE Visualization*, pages 65–72, 2005.

[48] Susumu Mori and Peter B. Barker. Diffusion magnetic resonance imaging: Its principle and applications. *THE ANATOMICAL RECORD (NEW ANAT.)*, 257:102–109, 1999.

[49] Susumu Mori, Barbara J. Crain, V. P. Chacko, and Peter C. M. Van Zijl. Three-dimensional tracking of axonal projections in the brain by magnetic resonance imaging. *Annals of Neurology*, 45(2):265–269, Feb 1999.

[50] Susumu Mori and Peter C. M. van Zijl. Fiber tracking: Principles and strategies – a technical review. *NMR in Biomedicine*, 15(7–8):468–480, 2002.

[51] Susumu Mori and Jiangyang Zhang. Principles of diffusion tensor imaging and its applications to basic neuroscience research. *Neuron*, 51:527–539, 2006.

[52] Andrew Y. Ng, Michael I. Jordan, and Yair Weiss. On spectral clustering: Analysis and an algorithm. In *Proc. 15th NIPS*, pages 849–856. MIT Press, 2001.

[53] Markus Nilsson, Jimmy Lätt, Emil Nordh, Ronnie Wirestam, Freddy Ståhlberg, and Sara Brockstedt. On the effects of a varied diffusion time in vivo: is the diffusion in white matter restricted? *Magnetic Resonance Imaging*, 27(2):176–187, 2009.

[54] Kenichi Oishi, Karl Zilles, Katrin Amunts, Andreia Faria, Hangyi Jiang, Xin Li, Kazi Akhter, Kegang Hua, Roger Woods, Arthur W. Toga, G. Bruce Pike, Pedro Rosa-Neto, Alan Evans, Jiangyang Zhang, Hao Huang, Michael I. Miller, Peter C.M. van Zijl, John Mazziotta, and Susumu Mori. Human brain white matter atlas: Identification and assignment of common anatomical structures in superficial white matter. *NeuroImage*, 43(3):447–457, 2008.

[55] Ofer Pasternak, Nir Sochen, and Yaniv Assaf. *Visualization and Processing of Tensor Fields*, chapter Variational Regularization of Multiple Diffusion Tensor Fields, pages 165–176. Springer, Berlin, 2005.

[56] M. Perrin, C. Poupon, Y. Cointepas, B. Rieul, N. Golestani, C. Pallier, D. Rivière, A. Constantinesco, D. Le Bihan, and J.-F. Mangin. Fiber tracking in q-ball fields using regularized particle trajectories. In *Proc. 19th IPMI*, volume 3565 of *Lecture Notes in Computer Science*, pages 52–63, Berlin, 2005. Springer.

[57] Carlo Pierpaoli and Peter J. Basser. Toward a quantitative assessment of diffusion anisotropy. *Magnetic Resonance in Medicine*, 36:893–906, Dec 1996.

[58] C. Poupon, C. A. Clark, V. Frouin, J. Rgis, I. Bloch, D. Le Bihan, and J. F. Mangin. Regularization of diffusion-based direction maps for the tracking of brain white matter fascicles. *NeuroImage*, 12(2):184–195, 2000.

[59] Arish A. Qazi, Alireza Radmanesh, Lauren O'Donnell, Gordon Kindlmann, Sharon Peled, Stephen Whalen, Carl-Fredrik Westin, and Alexandra J. Gobly. Resolving crossings in the corticospinal tract by two-tensor streamline tractography: Method and clinical assessment using fMRI. *NeuroImage*, 2009. in press.

[60] J. Ritchie. On the relation between fibre diameter and conduction velocity in myelinated nerve fibres. *Proc. Royal Society of London, Series B, Biological Sciences*, 217(1206):29–35, 1982.

[61] Denis Rivière, Jean-François Mangin, Dimitri Papadopoulos-Orfanos, Jean-Marc Martinez, Vincent Frouin, and Jean Régis. Automatic recognition of cortical sulci of the human brain using a congregation of neural networks. *Medical Image Analysis*, 6(2):77–92, 2002.

[62] P.E. Roland, Stefan Geyer, Katrin Amunts, Thorsten Schormann, Axel Schleicher, Aleksander Malikovic, and Karl Zilles. Cytoarchitectural maps of the human brain in standard anatomical space. *Human Brain Mapping*, 5(4):222–227, 1997.

[63] Peter Savadjiev, Jennifer S.W. Campbell, G. Bruce Pike, and Kaleem Siddiqi. 3D curve inference for diffusion MRI regularization and fibre tractography. *Medical Image Analysis*, 10(5):799–813, 2006.

[64] Jeremy D. Schmahmann and Deepak N. Pandya. *Fiber Pathways of the Brain.* Oxford University Press, New York, 2006.

[65] John Schreiner, Carlos E. Scheidegger, and Cláudio T. Silva. High-quality extraction of isosurfaces from regular and irregular grids. *IEEE Transactions onVisualization and Computer Graphics*, 12(5):1205–1212, 2006.

[66] David W. Shattuck, Stephanie R. Sandor-Leahy, Kirt A. Schaper, David A. Rottenberg, and Richard M. Leahy. Magnetic resonance image tissue classification using a partial volume model. *NeuroImage*, 13(5):856–876, 2001.

[67] Greg J. Stanisz, Graham A. Wright, R. Mark Henkelman, and Aaron Szafer. An analytical model of restricted diffusion in bovine optic nerve. *Magnetic Resonance in Medicine*, 37(1):103–111, 1997.

[68] E. O. Stejskal and J. E. Tanner. Spin diffusion measurements: Spin echoes in the presence of a time-dependent field gradient. *Journal of Chemical Physics*, 42(1):288–292, January 1965.

[69] J-Donald Tournier, Fernando Calamante, and Alan Connelly. Robust determination of the fibre orientation distribution in diffusion MRI: Non-negativity constrained super-resolved spherical deconvolution. *NeuroImage*, 35(4):1459–1472, 2007.

[70] David S. Tuch. Q-ball imaging. *Magnetic Resonance in Medicine*, 52(6):1358–1372, 2004.

[71] David S. Tuch, Timothy G. Reese, Mette R. Wiegell, and Van J. Wedeen. Diffusion MRI of complex neural architecture. *Neuron*, 40(5):885–895, 2003.

[72] G. Villarreal and C.Y. King. Brain imaging in posttraumatic stress disorder. *Seminars in Clinical Neuropsychiatry*, 6:131–145, Apr 2001.

[73] Ruopeng Wang, Thomas Benner, Alma Greg Sorensen, and Van Jay Wedeen. Diffusion Toolkit: A software package for diffusion imaging data processing and tractography. In *Proc. 15th ISMRM*, 2007.

[74] Zhizhou Wang, Baba C. Vemuri, Yunmei Chen, and Thomas H. Mareci. A constrained variational principle for direct estimation and smoothing of the diffusion tensor field from complex DWI. *IEEE Transactions on Medical Imaging*, 23(8):930–939, August 2004.

[75] V.J. Wedeen, R.P. Wang, J.D. Schmahmann, T. Benner, W.Y.I. Tseng, G. Dai, D.N. Pandya, P. Hagmann, H. D'Arceuil, and A.J. de Crespigny. Diffusion spectrum magnetic resonance imaging (DSI) tractography of crossing fibers. *NeuroImage*, 41(4):1267–1277, 2008.

[76] Song Zhang, Cagatay Demiralp, and David H. Laidlaw. Visualizing diffusion tensor MR images using streamtubes and streamsurfaces. *IEEE Transactions on Visualization and Computer Graphics*, 9(4):454–462, October 2003.

[77] Song Zhang and David H. Laidlaw. Hierarchical clustering of streamtubes. Technical Report CS-02-18, Brown University Computer Science Department, August 2002.

[78] Wenjin Zhou and David H. Laidlaw. An analytical model of diffusion and exchange of water in white matter from diffusion-MRI and its application in measuring axon radii. In *Proc. 17th ISMRM*, page 263, 2009.

[79] Z. Zuo, X. Wang, N. Chen, J. Luo, Y. Zhuo, D. Shen, K. Li, and R. Xue. Establishing probabilistic chinese human brain templates using HAMMER elastic registration algorithm. In *Proc. 17th ISMRM*, 2009.